



Original Article

Preparation and Characterization of SrFe₁₂O₁₉/rGO and SrFe₁₂O₁₉/SiO₂ -based Composite Materials for Enhancement of Microwave Absorption Properties

Tran Thi Viet Nga^{1,*}, Nguyen Van Quang², To Thanh Loan¹

¹*School of Materials Science and Engineering, University of Science and Technology,
1 Dai Co Viet, Hanoi, Vietnam*

²*School of Engineering Physic, Hanoi University of Science and Technology,
1 Dai Co Viet, Hanoi, Vietnam*

Received 27 July 2024

Revised 21 August 2024; Accepted 10 December 2024

Abstract: In this work, we synthesized and investigated the microwave absorption properties of SrFe₁₂O₁₉, SrFe₁₂O₁₉/rGO and SrFe₁₂O₁₉/SiO₂ materials prepared by chemical method. The phase structure, surface morphology, magnetic properties, and electromagnetic wave absorption characteristics of the samples were studied and compared. The SEM images of SrFe₁₂O₁₉/rGO sample showed a good stability in the distribution and dispersion of SrFe₁₂O₁₉ nanoparticles on rGO sheets. For SrFe₁₂O₁₉/SiO₂ composite samples, it is shown that SiO₂ coating is enwrapped on the SrFe₁₂O₁₉ surface, forming SrFe₁₂O₁₉/SiO₂ nanocomposites with core-shell structure. The average particle size was found in the range of 60 – 120 nm. The composite SrFe₁₂O₁₉/rGO sample exhibited a minimum reflection loss reached -56.21 dB at 18 GHz with EAB of 12 GHz with a thickness of 3.5 mm. One can suggest that composite SrFe₁₂O₁₉/rGO materials possessing a best performance in both reflectivity and bandwidth can be used in the field of microwave absorption.

Keywords: Microwave absorption properties, hexaferrite, rGO, SiO₂.

1. Introduction

Nowadays, the rapid advancement of technology has enabled the development of new telecommunication and electronic devices, which are used in the fields of military, commercial activities and medicine, etc. Therefore, electromagnetic (EM) wave pollution has become a serious issue in both

* Corresponding author.

E-mail address: vietnga@itims.edu.vn

<https://doi.org/10.25073/2588-1124/vnumap.4957>

civilian and military sectors. EM wave pollution not only threatens information security but also causes numerous health problems for humans. Thus, the harmful effects of EM waves, especially in the field of EM radiation in military areas, must be mitigated. In recent years, thin and lightweight electromagnetic wave absorbing materials that exhibit broad bandwidth and high absorption performance have received more attention. Studies have shown that traditional wave-absorbing materials with a single structural phase and single component hardly meet above mentioned requirements [1-6]. In order to overcome these difficulties, many researchers have made efforts to develop materials comprising two or three components. Among them, composite materials that combine magnetic and dielectric materials are promising candidates for improving wave absorption performance [2, 6-13]. Hexagonal ferrites have been extensively studied regarding magnetic loss because of their high complex permeability, high saturation magnetization, and low-cost production. Furthermore, hexagonal ferrite materials with flake-like structures can produce a strong interfacial polarization and possess enhanced microwave absorption properties because of the large surface areas [14]. Combining hexaferrite materials with dielectric materials gives a positive effect on the enhancing absorption performance and broadening the absorption bandwidth due to improved impedance matching and interfacial polarization [15]. The minimum reflection loss (RL) of - 52.21 dB at a frequency of 10.72 GHz with a thickness of 2.1 mm was obtained for the reduced graphene oxide (rGO)/BaFe₁₂O₁₉ composite [10]. While the minimum RL of SrFe₁₂O₁₉/G composites with the thickness of 3.0 mm reached - 34.8 dB at 13.6 GHz, and the effective absorption bandwidth ($RL < -10$ dB) was of 5.7 GHz. However, the minimum RL of the SrFe₁₂O₁₉ particles reached - only 13.5 dB, and the effective absorption bandwidth was of 4.6 GHz. Optimization of the samples thickness towards microwave absorption enhancement in three-layer absorber based on SrFe₁₂O₁₉, SiO₂@S SrFe₁₂O₁₉ and MWCNTs@ SrFe₁₂O₁₉ nanocomposites has also been reported [16]. The minimum RL is reached to - 42 dB at 9.5 GHz with 4.2 GHz effective bandwidth which composed of three distinct resonance peaks at 9.5, 10.5 and 11.5 GHz.

In this work, we focused on studying the microwave absorption capabilities of SrFe₁₂O₁₉, SrFe₁₂O₁₉/rGO and SrFe₁₂O₁₉/SiO₂ materials. The samples can have both the good electrical conductivities and electromagnetic properties, in order to significantly improve the microwave absorption performance of the nanocomposite.

2. Experimental

2.1. Synthesis of samples

SrFe₁₂O₁₉ particles were synthesized by sol-gel method with following technical parameters: Fe/Sr molar ratio is of 10.5, pH is of 1.0, the molar ratio of (Sr²⁺+Fe³⁺)/ C₃H₄(OH)(COOH)₃ is of 1/3, and the evaporated temperature is of 80 °C [16]. Fe(NO₃)₃ (1 M) and Sr(NO₃)₃ (1 M) were dissolved in deionized water and then mixed in a Fe/Sr ratio of 10.5. Citric acid was added into the solution at a fixed [Sr²⁺+Fe³⁺]: C₃H₄(OH)(COOH)₃ molar ratio of 1/3. Then, the mixture was gelation at 80 °C with a brown color. The samples were dried at 100 °C for 24 h and then heated at 450 °C for 2 h to remove all residuals. To obtain the hexagonal ferrite phase, the product was calcined in air at 950 °C for 2 h. Synthesis of SrFe₁₂O₁₉/rGO was carried-out two steps as follows.

Step 1: GO was synthesized using the modified Hummer's method [17].

Step 2: GO sheets were dispersed in a mixture of deionized water and ethanol; and sonicated for 60 min, to stabilize the GO. Then, SrFe₁₂O₁₉ nanoparticles were added to the dispersed solution with the weight ratio SrFe₁₂O₁₉/rGO of 9/1 and the mixture was stirred for 24 h. The resulting nanocomposite was separated magnetically and dried at 80 °C overnight in air.

SrFe₁₂O₁₉/SiO₂ nanoparticles were synthesized via a modified Stöber method. Firstly, the surface of 1.0 g of SrFe₁₂O₁₉ particles will be modified by dispersing them in 20 ml ethanol ultrasonically for 2 h. After that 5 ml of deionized water and 1 ml of tetrathyl orthosilicate (TEOS) were added to the solution and sonicated for 30 min. Then, 0.2 ml of NH₄OH was added into the mixture under stirring for 8 h at room temperature. Finally, the products were washed with deionized water and dried at 60 °C for 24 h.

2.2. Characterization

Experiment results indicated that the samples combined with paraffin have a mass concentration of 30%, displaying promising blending characteristics. Upon undergoing toroidal molding, the mixtures acquired an internal diameter of 3.04 mm and an external diameter of 7.00 mm. The microwave absorption properties were studied by using the Keysight PNA-X N5242A vector network analyzer. The characteristics of the microwave absorption were determined by employing the transmission line method. The following equations furnished an all-encompassing understanding of *RL* [18]:

$$RL(dB) = 20 \cdot \log \left| \frac{Z_{in} - Z_0}{Z_{in} + Z_0} \right|, \quad (1)$$

$$Z_{in} = Z_0 \sqrt{\frac{\mu_r}{\varepsilon_r}} \tanh \left(j \frac{2\pi f d}{c} \sqrt{\mu_r \varepsilon_r} \right). \quad (2)$$

In analyzing absorber input impedance (Z_{in}), intrinsic impedance of free space (Z_0), the intricate relative permittivity (ε_r) and permeability (μ_r) were considered. The thickness of the samples (d), frequency of the incident light (f), and velocity of light propagation in a vacuum (c) are the additional factors to be considered in this work.

The crystalline structure the samples were identified via X-ray powder diffraction (XRD) using a Siemens D5000 diffractometer (Cu-K α radiation; $\lambda = 1.54056 \text{ \AA}$). The morphology and the particle size were observed via scanning electron microscopy (SEM; JEOL-JSM 7600F). The Raman spectra were obtained using a Raman spectrometer in the 200–2000 cm⁻¹ range. The chemical groups were analyzed using Fourier transform infrared (FTIR) spectroscopy measurement (Nicolet 6700) in the range of 400 cm⁻¹ to 4,000 cm⁻¹. The magnetic properties were measured using a vibrating sample magnetometer (Lakeshore 7410) with applied magnetic fields of up to 15 kOe.

3. Results and Discussion

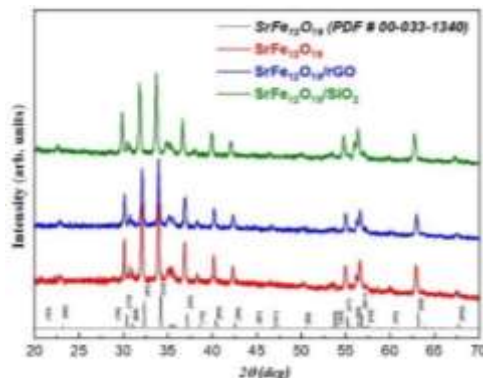


Figure 1. XRD patterns of SrFe₁₂O₁₉, SrFe₁₂O₁₉/rGO and SrFe₁₂O₁₉/SiO₂ samples.

Fig. 1 shows the XRD patterns of $\text{SrFe}_{12}\text{O}_{19}$, $\text{SrFe}_{12}\text{O}_{19}/\text{rGO}$, $\text{SrFe}_{12}\text{O}_{19}/\text{SiO}_2$ samples. For all samples, all detected diffraction peaks correspond to those of strontium hexaferrite (PDF file number 00-033-1340). After combining with GO and SiO_2 , we did not observe any characteristic peaks of SiO_2 and GO. This may be attributed to the weight percentage of GO (10%) is much smaller than $\text{SrFe}_{12}\text{O}_{19}$ (90%) [17] and SiO_2 formed an amorphous manner in the composited samples [19]. Figure 2 shows FTIR spectra of $\text{SrFe}_{12}\text{O}_{19}/\text{rGO}$ and $\text{SrFe}_{12}\text{O}_{19}/\text{SiO}_2$ samples, the samples show a peak at 582 cm^{-1} corresponding to the metal-oxide bonding in strontium hexaferrite structure [20-22]. The spectrum of $\text{SrFe}_{12}\text{O}_{19}/\text{rGO}$ sample includes all the peaks of pure $\text{SrFe}_{12}\text{O}_{19}$ and additional peaks at 3460 cm^{-1} , 1630 cm^{-1} , 1215 cm^{-1} and 1090 cm^{-1} belong to the stretching mode of OH group, C=C stretching mode, stretching of C-OH in COOH group, and C-O-C stretching vibrations, respectively [22-24]. While the spectrum of the $\text{SrFe}_{12}\text{O}_{19}/\text{SiO}_2$ sample exhibits distinctive peaks corresponding to SiO_2 bonds (Si-O and Si-O-Si) in the range of 800 cm^{-1} to 1221 cm^{-1} , the vibration at a wavenumber of 1624 cm^{-1} indicates the presence of Si-OH bonds [21, 22]. These results confirm the presence of both rGO and SiO_2 in the composite material.

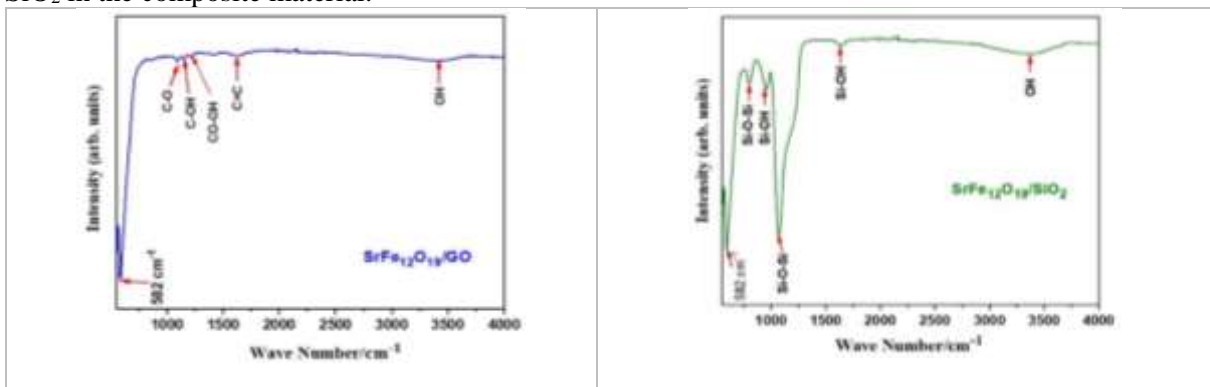


Figure 2. FTIR analysis of $\text{SrFe}_{12}\text{O}_{19}/\text{rGO}$ and $\text{SrFe}_{12}\text{O}_{19}/\text{SiO}_2$ composite samples.

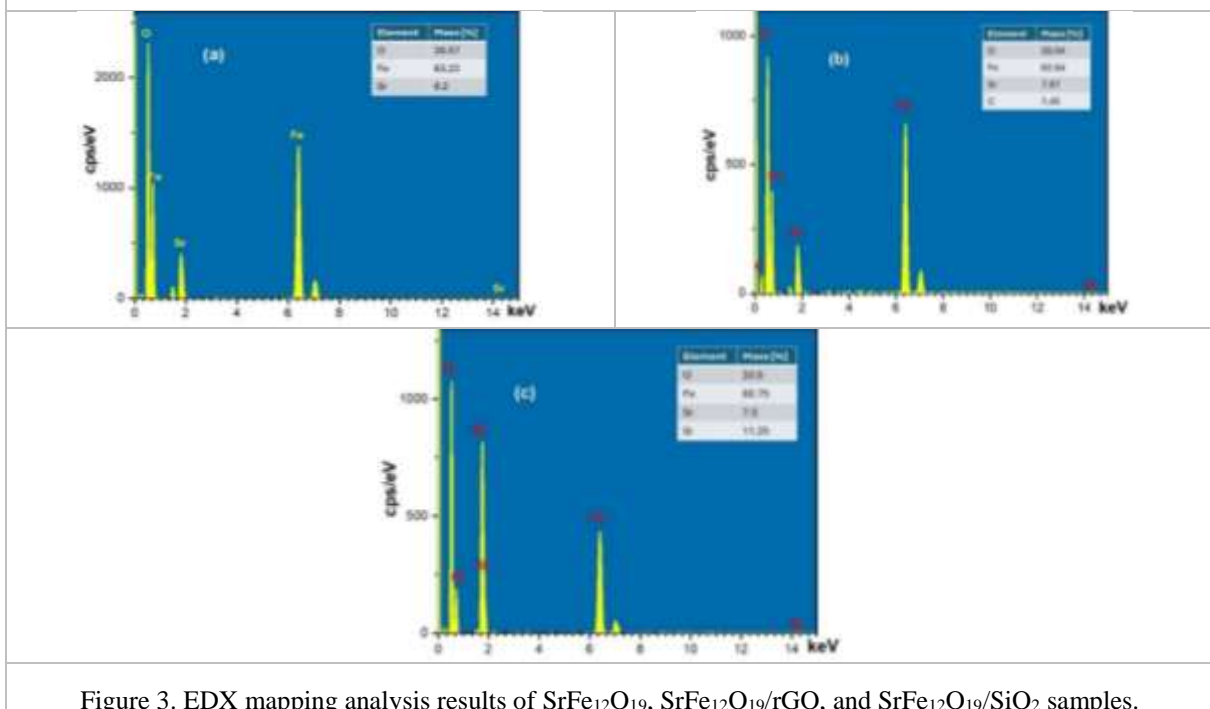


Figure 3. EDX mapping analysis results of $\text{SrFe}_{12}\text{O}_{19}$, $\text{SrFe}_{12}\text{O}_{19}/\text{rGO}$, and $\text{SrFe}_{12}\text{O}_{19}/\text{SiO}_2$ samples.

The EDX spectra of pure $\text{SrFe}_{12}\text{O}_{19}$, $\text{SrFe}_{12}\text{O}_{19}/\text{rGO}$ and $\text{SrFe}_{12}\text{O}_{19}/\text{SiO}_2$ samples are presented in Fig. 3. One can see that the pure $\text{SrFe}_{12}\text{O}_{19}$ sample consists of Sr, Fe and O elements (Fig. 3a), the ratio of Sr, Fe and O in this sample was determined to be of 1: 12.5: 19.2. While for the $\text{SrFe}_{12}\text{O}_{19}/\text{rGO}$ and $\text{SrFe}_{12}\text{O}_{19}/\text{SiO}_2$ composite samples (Fig. 3b, c), except for Sr, Fe and O, other peaks such as C and Si also exist. These results confirmed graphene and SiO_2 phases in the composite samples. The XRD, FTIR and EDS have proved the successful synthesis of $\text{SrFe}_{12}\text{O}_{19}/\text{rGO}$ and $\text{SrFe}_{12}\text{O}_{19}/\text{SiO}_2$ composite samples.

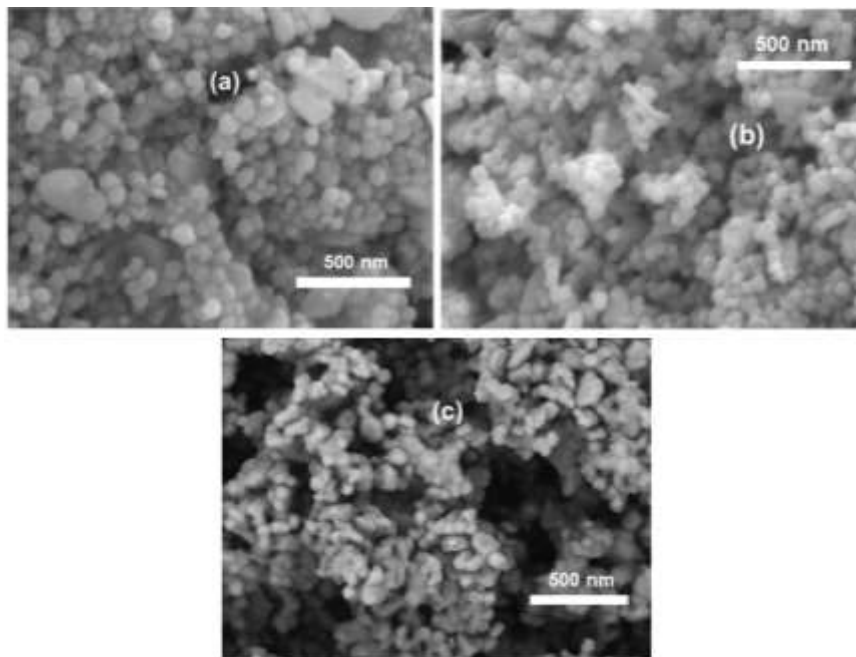


Figure 4. FESEM micrographs of $\text{SrFe}_{12}\text{O}_{19}$, $\text{SrFe}_{12}\text{O}_{19}/\text{rGO}$, and $\text{SrFe}_{12}\text{O}_{19}/\text{SiO}_2$ samples.

Figure 4 presents scanning electron microscopy (SEM) micrographs illustrating the morphology of $\text{SrFe}_{12}\text{O}_{19}$, $\text{SrFe}_{12}\text{O}_{19}/\text{rGO}$ and $\text{SrFe}_{12}\text{O}_{19}/\text{SiO}_2$ nanocomposite samples. $\text{SrFe}_{12}\text{O}_{19}$ particles exhibited a hexagonal platelet shape and a smooth surface. The average particle size of these plate-like $\text{SrFe}_{12}\text{O}_{19}$ was evenly distributed in the range of 50-100 nm. The FESEM images of $\text{SrFe}_{12}\text{O}_{19}/\text{rGO}$ sample showed good stability in the distribution and dispersion of $\text{SrFe}_{12}\text{O}_{19}$ nanoparticles on rGO sheets. For $\text{SrFe}_{12}\text{O}_{19}/\text{SiO}_2$ composite sample, one can clearly see that SiO_2 coating is enwrapped on the $\text{SrFe}_{12}\text{O}_{19}$ surface forming $\text{SrFe}_{12}\text{O}_{19}/\text{SiO}_2$ nanocomposites with core-shell structure. The average particle size was distributed in the range of $60 \div 120$ nm.

Figure 5 compares the hysteresis loops of three samples at room temperature. One can see that all samples exhibit a hardmagnetic behavior, with coercivity H_C reaching 6.9 kOe. The saturation magnetization (M_s) of the $\text{SrFe}_{12}\text{O}_{19}$, $\text{SrFe}_{12}\text{O}_{19}/\text{rGO}$, and $\text{SrFe}_{12}\text{O}_{19}/\text{SiO}_2$ are of 59.4, 57.6 and 40.5 emu/g, respectively. This is due to the presence of nonmagnetic contents (rGO and SiO_2).

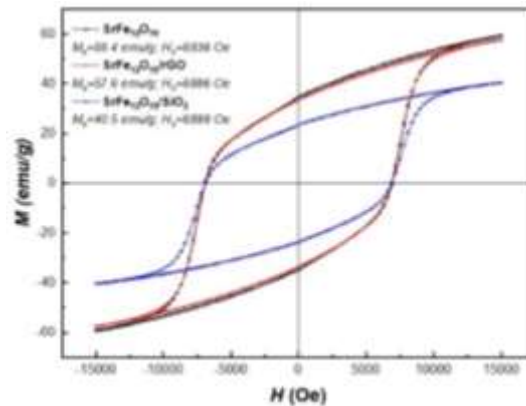


Figure 5. Hysteresis loops of SrFe₁₂O₁₉, SrFe₁₂O₁₉/rGO, and SrFe₁₂O₁₉/SiO₂ samples.

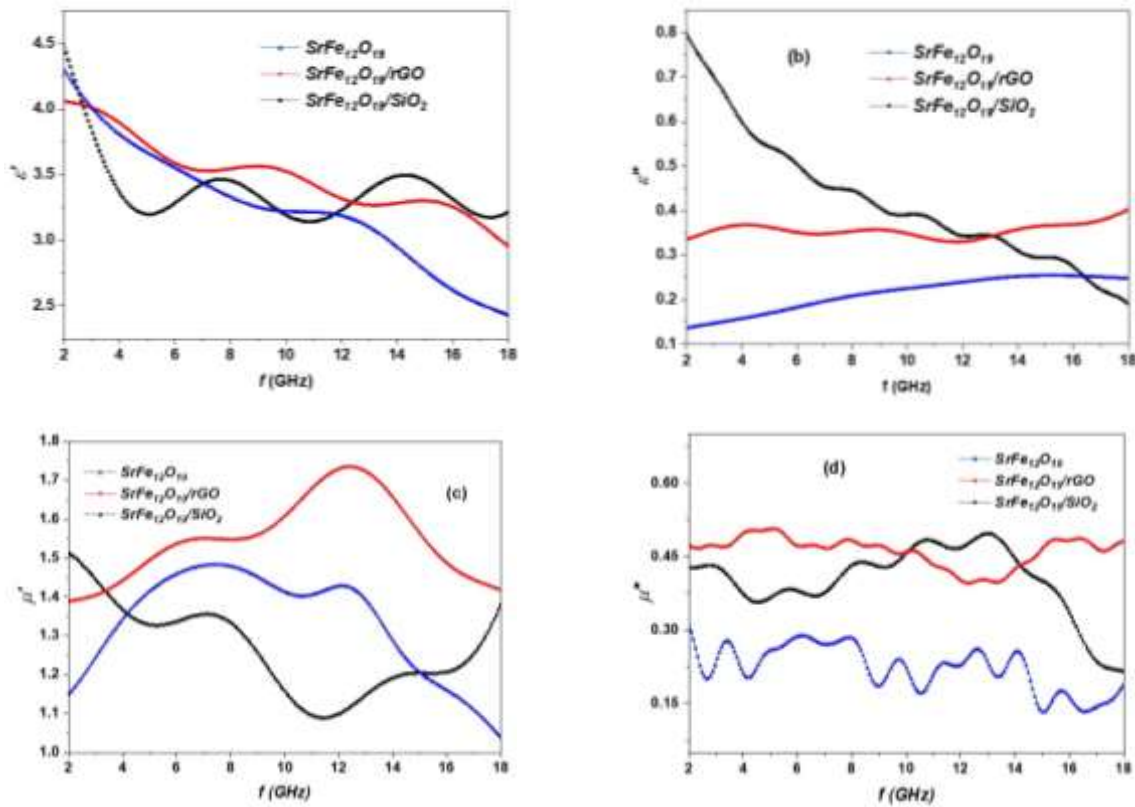


Figure 6. Frequency dependence of the real (a, c) and imaginary (b, d) parts of complex permittivity (ϵ) and complex permeability (μ), respectively.

Fig. 6 shows the relationship between the real and imaginary components of the complex permittivity (ϵ), complex permeability (μ) and their frequency-dependent properties. The real parts of complex permittivity (ϵ') and permeability (μ') represent the storage of electric and magnetic energy, respectively. The imaginary parts of complex permittivity (ϵ'') and permeability (μ'') are characteristics of the loss of electric and magnetic energy, respectively. The real (ϵ') components of complex

permittivity (ϵ) show a decrease with increasing frequency. In the low frequency, the ϵ' of SrFe₁₂O₁₉/SiO₂ sample decrease with increasing frequency and then fluctuates between 3.2 and 3.5. ϵ'' of SrFe₁₂O₁₉ and SrFe₁₂O₁₉/rGO samples go up slightly with frequency, where ϵ'' of SrFe₁₂O₁₉/SiO₂ sample go up significantly with frequency. As shown in Figs. 6c and 6d, μ' and μ'' represent a complicated insituation with an amount of diffraction peak which related magnetism behavior inside a structure. μ'' of SrFe₁₂O₁₉/rGO and SrFe₁₂O₁₉/SiO₂ samples are larger than the one of SrFe₁₂O₁₉ sample, this indicated an improvement in the magnetic loss of materials. The enhanced magnetic properties, specifically the real and imaginary parts of the complex permeability of SrFe₁₂O₁₉ @rGO and SrFe₁₂O₁₉/SiO₂ compared to SrFe₁₂O₁₉ can be attributed to the effect of addition of rGO and SiO₂. The addition of rGO and SiO₂ makes the increase of the surface area and more interaction sites introduced. For all parameters, the real part is largeher than the imaginary part. This indicates a tendency to store energy in these materials.

The dielectric ($\tan\delta_\epsilon = \epsilon''/\epsilon'$) and magnetic loss tangent ($\tan\delta_\mu = \mu''/\mu'$) were determined. Fig. 7 shows the dependence of $\tan\delta_\epsilon$ and $\tan\delta_\mu$ on frequency (f). The dielectric and magnetic loss tangent signifies the extent to which microwaves lose energy. The order of the dielectric loss between 2 and 12 GHz of frequency was obtained for SrFe₁₂O₁₉/SiO₂, SrFe₁₂O₁₉/rGO and SrFe₁₂O₁₉ samples. Introducing rGO and SiO₂ to SrFe₁₂O₁₉ system results in the decrease of the resistivity, leading to the increase in the dielectric loss. However, within the frequency range of 14-18 GHz, the dielectric loss of SrFe₁₂O₁₉/rGO and SrFe₁₂O₁₉ increases, surpassing the dielectric loss of SrFe₁₂O₁₉/SiO₂ sample. The magnetic losses also show a similar trend with the frequency range from 2 GHz to 18 GHz. The loss tangent values of all samples are larger than the dielectric loss tangent values over the entire frequency range, suggesting that the magnetic loss dominates microwave absorption.

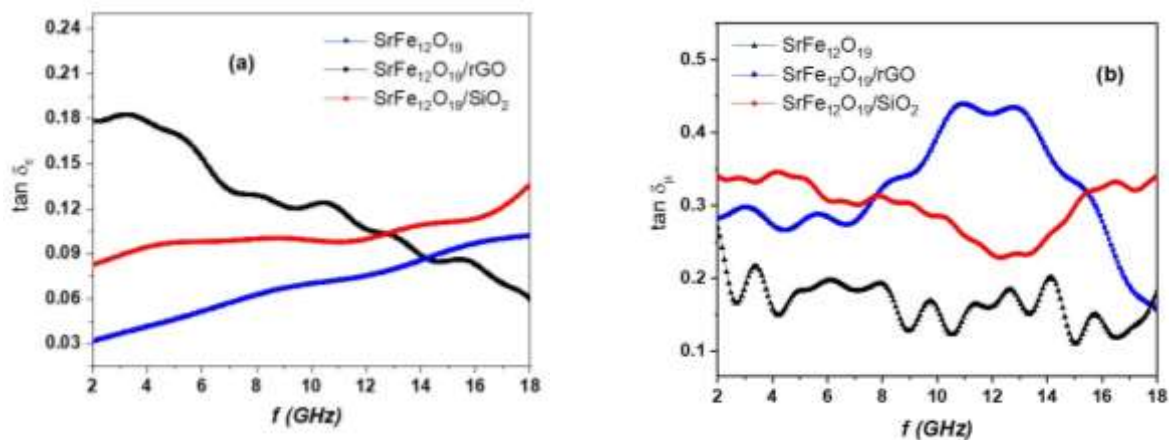


Figure 7. Frequency dependence of the dielectric ($\tan\delta_\epsilon = \epsilon''/\epsilon'$) (a) and magnetic loss tangent ($\tan\delta_\mu = \mu''/\mu'$) (b), respectively.

Usually, when the reflection loss (RL) reaches values of -10 dB and -20 dB, it indicates that a significant amount of electromagnetic waves (EMW) can be absorbed. Typically, when the reflection loss is below -10 dB, it indicates that more than 90% of the microwave is absorbed. Only absorbents with a reflection loss below -10 dB are suitable for practical use. As a result, the frequency range that shows RL values below -10 dB can be categorized as an electromagnetic absorption band (EAB).

Fig. 8 displays the computed reflection loss values for the SrFe₁₂O₁₉, SrFe₁₂O₁₉/rGO and SrFe₁₂O₁₉/SiO₂ materials. The layer thickness investigated ranges from 1.5 to 5.0 mm, and the frequency

range analyzed is from 2 to 18 GHz. The RL_{\min} value of $SrFe_{12}O_{19}$ is -43.55 at 13.2 GHz with an EAB of 13.2 GHz for thicknesses of 5.0 mm. The $SrFe_{12}O_{19}/rGO$ sample achieves lower RL with thinner thickness. The RL_{\min} of $SrFe_{12}O_{19}/rGO$ reaches -56.21 dB at 18 GHz with EAB of 12 GHz for thickness of 3.5 mm. Whereas $SrFe_{12}O_{19}/SiO_2$ shows RL_{\min} of -46.47 dB at 13.92 GHz with an EAB of 9.2 GHz with test thickness of 2.0 mm. Thus, the rational introduction of graphene layer and tiny silica particles contributed to the improved microwave absorption performance. On the other hand, all samples show EAB (reaching more than 13 GHz) indicating a remarkable improvement in microwave absorption ability.

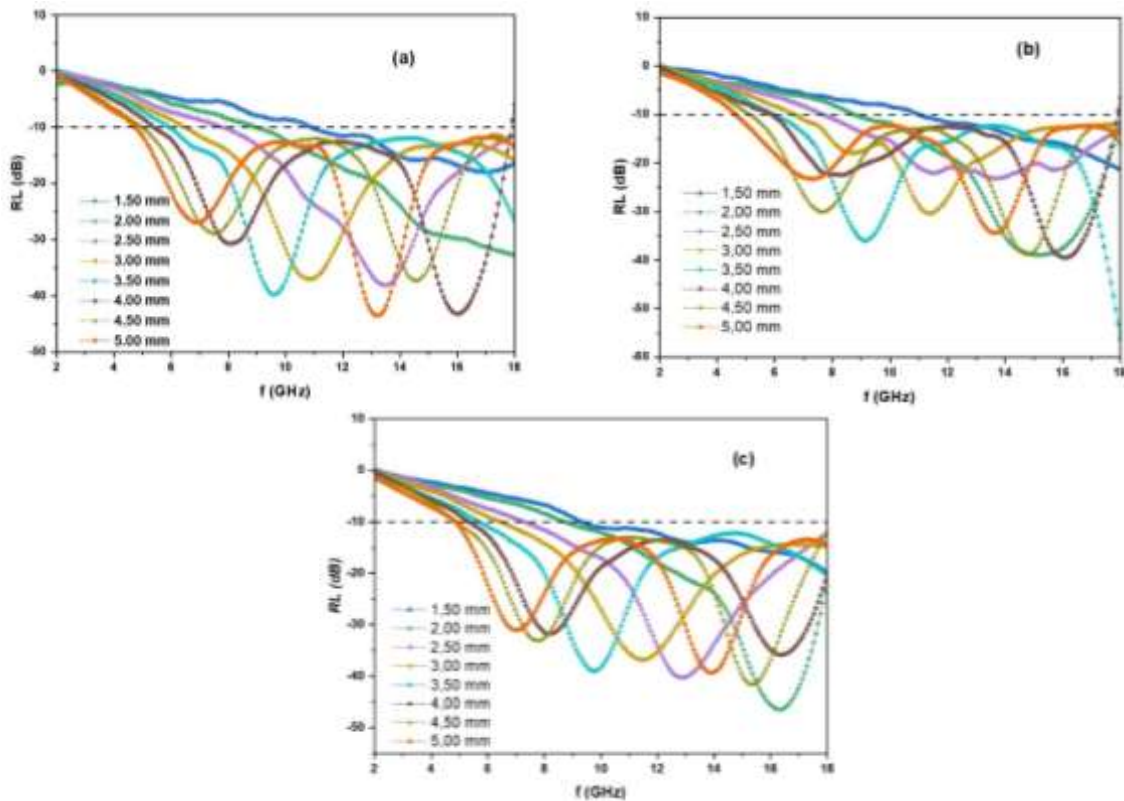


Figure 8. The reflection losses of (a) $SrFe_{12}O_{19}$, (b) $SrFe_{12}O_{19}/rGO$ and (c) $SrFe_{12}O_{19}/SiO_2$ samples.

4. Conclusion

$SrFe_{12}O_{19}/rGO$ and $SrFe_{12}O_{19}/SiO_2$ samples were successfully prepared by chemical methods. The obtained results show that the $SrFe_{12}O_{19}$ nanoparticles were wrapped by rGO sheet and covered by tiny SiO_2 particles that exhibited excellent microwave absorption performance in combination with a wide absorption band and enhanced reflection loss. Notably, with a thickness of 3.5 mm, the minimum RL of $SrFe_{12}O_{19}/rGO$ sample reaches -56.21 dB at 18 GHz which lower 20% than that of $SrFe_{12}O_{19}/SiO_2$ sample. The analysis results reveal that the excellent microwave absorption performance of the samples is attributed to the multi-component structure, suitable nature of materials. In addition, the synthesis process of the samples is simple, thus easy to operate. The obtained results of this work suggests new approaches for designing broadband and highly efficient microwave absorbers.

Acknowledgments

This research is funded by Hanoi University of Science and Technology (HUST) under project number T2022-PC-090.

Reference

- [1] X. Huang, J. Zhang, Z. Liu, T. Sang, B. Song, H. Zhu, C. Wong, Facile Preparation and Microwave Absorption Properties of Porous Hollow BaFe₁₂O₁₉/CoFe₂O₄ Composite Microrods, *J. Alloys Compd.*, Vol. 648, 2015, pp. 1072-1075, <https://doi.org/10.1016/j.jallcom.2015.07.073>.
- [2] S. Jiao, M. Wu, X. Yu, H. Hu, Z. Bai, P. Dai, T. Jiang, H. Bi, G. Li, RGO/BaFe₁₂O₁₉/Fe₃O₄ Nanocomposite as Microwave Absorbent with Lamellar Structures and Improved Polarization Interfaces, *Mater. Res. Bull.*, Vol. 108, 2018, pp. 89-95, <https://doi.org/10.1016/j.materresbull.2018.08.014>.
- [3] S. Kolev, T. Koutzarova, A. Yanev, C. Ghelev, I. Nedkov, Microwave Properties of Polymer Composites Containing Combinations of Micro- and Nano-sized Magnetic Fillers, *J. Nanosci. Nanotechnol.*, Vol. 8, 2008, pp. 650-654, <https://doi.org/10.1166/jnn.2008.B069>.
- [4] S. H. Hosseini, P. Zamani, Preparation of Thermal Infrared and Microwave Absorber Using SrTiO₃/BaFe₁₂O₁₉/polyaniline Nanocomposites, *J. Magn. Magn. Mater.*, Vol. 397, 2016, pp. 205-212, <https://doi.org/10.1016/j.jmmm.2015.08.105>.
- [5] A. A. H. Hernández, G. A. Á. Romero, A. C. Ovando, Y. M. Tolentino, E. C. López, C. A. G. Vidal, M. E. P. Hernández, Optimization of Microwave-Solvothermal Synthesis of Fe₃O₄ Nanoparticles, Coating, Modification and Characterization, *Mater. Chem. Phys.*, Vol. 205, 2018, pp. 113-119, <https://doi.org/10.1016/j.matchemphys.2017.11.009>.
- [6] H. Yang, T. Ye, Y. Lin, M. Liu, Preparation and Microwave Absorption Property of Graphene/BaFe₁₂O₁₉/CoFe₂O₄ Nanocomposite, *Appl. Surf. Sci.*, Vol. 357, 2015, pp. 1289-1293, <https://doi.org/10.1016/j.apsusc.2015.09.147>.
- [7] N. Li, H. L. Jiang, X. Wang, X. Wang, G. Xu, B. Zhang, L. Wang, R. S. Zhao, J. M. Lin, Recent Advances in Graphene-based Magnetic Composites for Magnetic Solid-phase Extraction, *TrAC - Trends Anal. Chem.*, Vol. 102, 2018, pp. 60-74, <https://doi.org/10.1016/j.trac.2018.01.009>.
- [8] J. Luo, P. Shen, W. Yao, C. Jiang, J. Xu, Synthesis, Characterization and Microwave Absorption Properties of Reduced Graphene Oxide/Strontium Ferrite/Polyaniline Nanocomposites, *Nanoscale Res. Lett.*, Vol. 11, 2016, pp. 1-14, <https://doi.org/10.1186/s11671-016-1340-x>.
- [9] W. Chen, Q. Liu, X. Zhu, M. Fu, One-step in Situ Synthesis of Strontium Ferrites and Strontium Ferrites/graphene Composites as Microwave Absorbing Materials, *RSC Adv.*, Vol. 7, 2017, pp. 40650-40657, <https://doi.org/10.1039/c7ra05700h>.
- [10] S. Goel, A. Garg, R. K. Gupta, A. Dubey, N. E. Prasad, S. Tyagi, Development of RGO/BaFe₁₂O₁₉-based Composite Medium for Improved Microwave Absorption Applications, *Appl. Phys. A Mater. Sci. Process.*, Vol. 126, 2020, pp. 1-11, <https://doi.org/10.1007/s00339-020-03613-3>.
- [11] S. Jiao, M. Wu, X. Yu, H. Hu, Z. Bai, P. Dai, T. Jiang, H. Bi, G. Li, RGO/BaFe₁₂O₁₉/Fe₃O₄ Nanocomposite as Microwave Absorbent with Lamellar Structures and Improved Polarization Interfaces, *Mater. Res. Bull.*, Vol. 108, 2018, pp. 89-95, <https://doi.org/10.1016/j.materresbull.2018.08.014>.
- [12] Y. T. Ng, W. Kong, S. Appadu, I. Kong, Microwave Absorption Properties of Fe₃O₄-Graphene Nanohybrids, *Solid State Phenom.*, Vol. 268 SSP, 2017, pp. 297-301, <https://doi.org/10.4028/www.scientific.net/SSP.268.297>.
- [13] S. Mallesh, W. Jang, K. H. Kim, Facile Synthesis of Cube-like Fe₃O₄-Graphene Oxide Nanocomposites with Excellent Microwave Absorption Performance, *Phys. Lett. Sect. A Gen. At. Solid State Phys.*, Vol. 389, 2021, pp. 10042-10047, <https://doi.org/10.1016/j.physleta.2020.127069>.
- [14] Y. Wang, Y. Huang, Q. Wang, Q. He, L. Chen, Preparation and Electromagnetic Properties of Polyaniline(polypyrrole)- BaFe₁₂O₁₉/Ni_{0.8}Zn_{0.2}Fe₂O₄ Ferrite Nanocomposites, *Appl. Surf. Sci.*, Vol. 259, 2012, pp. 486-493, <https://doi.org/10.1016/j.apsusc.2012.07.072>.
- [15] Z. Durmus, H. Kavas, A. Durmus, B. Aktaş, Synthesis and Micro-structural Characterization of Graphene/strontium Hexaferrite (SrFe₁₂O₁₉) Nanocomposites, *Mater. Chem. Phys.*, Vol. 163, 2015, pp. 439-445, <https://doi.org/10.1016/j.matchemphys.2015.07.063>.

- [16] X. Zhu, X. Wang, K. Liu, H. Yuan, R. Boudaghi, M. N. Akhtar, Thickness Optimization towards Microwave Absorption Enhancement in Three-layer Absorber Based on $\text{SrFe}_{12}\text{O}_{19}$, $\text{SiO}_2@ \text{SrFe}_{12}\text{O}_{19}$ and $\text{MWCNTs}@ \text{SrFe}_{12}\text{O}_{19}$ Nanocomposites, *J. Alloys Compd.*, Vol. 873, 2021, pp. 1-11, <https://doi.org/10.1016/j.jallcom.2021.159818>.
- [17] M. D. Dung, T. T. V. Nga, N. T. Lan, N. K. Thanh, Adsorption Behavior and Mechanism of As(V) on Magnetic Fe_3O_4 -graphene Oxide (GO) Nanohybrid Composite Material, *Anal. Sci.*, Vol. 38, 2022, pp. 427-436, <https://doi.org/10.1007/s44211-022-00064-z>.
- [18] M. F. Elmahaishi, R. S. Azis, I. Ismail, F. D. Muhammad, A Review on Electromagnetic Microwave Absorption Properties: Their Materials and Performance, *J. Mater. Res. Technol.*, Vol. 20, 2022, pp. 2188-2220, <https://doi.org/10.1016/j.jmrt.2022.07.140>.
- [19] M. M. Baig, E. Pervaiz, M. Azad, Z. Jahan, M. B. K. Niazi, S. M. Baig, $\text{NiFe}_2\text{O}_4/\text{SiO}_2$ Nanostructures as A Potential Electrode Material for High Rated Supercapacitors, *Ceram. Int.*, Vol. 47, 2021, pp. 12557-12566, <https://doi.org/10.1016/j.ceramint.2021.01.113>.
- [20] Z. H. Karahroudi, K. Hedayati, M. Goodarzi, Green Synthesis and Characterization of Hexaferrite Strontium-Perovskite Strontium Photocatalyst Nanocomposites, *Main Gr. Met. Chem.*, Vol. 43, 2020, pp. 26-42, <https://doi.org/10.1515/mgmc-2020-0004>.
- [21] F. Bavarsiha, M. Rajabi, M. M. Pour, Synthesis of $\text{SrFe}_{12}\text{O}_{19}/\text{SiO}_2/\text{TiO}_2$ Composites with Core/shell/shell Nanostructure and Evaluation of Their Photo-catalytic Efficiency for Degradation of Methylene Blue, *J. Mater. Sci. Mater. Electron.*, Vol. 29, 2018, pp. 1877-1887, <https://doi.org/10.1007/s10854-017-8098-5>.
- [22] K. Mohammadi, M. Sadeghi, R. Azimirad, Facile Synthesis of $\text{SrFe}_{12}\text{O}_{19}$ Nanoparticles and Its Photocatalyst Application, *J. Mater. Sci. Mater. Electron.*, Vol. 28, 2017, pp. 10042-10047, <https://doi.org/10.1007/s10854-017-6763-3>.
- [23] T. T. V. Nga, N. T. Lan, Fabrication and Exchange-spring Properties of $\text{SrFe}_{12}\text{O}_{19}@ \text{Fe}_3\text{O}_4$ Nanocomposites with Core-shell Structure, *Mater. Chem. Phys.*, Vol. 251, 2020, <https://doi.org/10.1016/j.matchemphys.2020.123084>.
- [24] T. T. V. Nga, N. V. Quang, T. T. Loan, Study on Microwave Absorption Performance of Submicron $\text{SrFe}_{12}\text{O}_{19}$ Particles Prepared by Hydrothermal Method, *VNU Journal of Science: Mathematics – Physics*, Vol. 40, No. 1, 2024, pp. 10-17, <https://doi.org/10.25073/2588-1124/vnumap.4851>.